International Journal of Hydrogen Energy 178 (2025) 151442

Contents lists available at ScienceDirect

International Journal of Hydrogen Energy

journal homepage: www.elsevier.com/locate/he

Sodium-decorated PHE-graphene as a high-capacity hydrogen storage material: A first-principles investigation

José A.S. Laranjeira [a,*], Nicolas F. Martins [a], Kleuton A.L. Lima [b,c], Luiz A. Ribeiro Junior [b,c], Marcelo L. Pereira Junior [d], Julio R. Sambrano [a], Xihao Chen [e,*]

[a] Modeling and Molecular Simulation Group, São Paulo State University (UNESP), School of Sciences, Bauru, 17033-360, SP, Brazil
[b] Institute of Physics, University of Brasília, Brasília, 70910-900, DF, Brazil
[c] Computational Materials Laboratory, LCCMat, Institute of Physics, University of Brasília, Brasília, 70910-900, DF, Brazil
[d] University of Brasília, College of Technology, Department of Electrical Engineering, Brasília, 70910-900, DF, Brazil
[e] School of Materials Science and Engineering, Chongqing University of Arts and Sciences, Chongqing, 402160, China

ARTICLE INFO

Keywords:
Hydrogen storage
PHE-graphene
Alkali metal decoration
Density functional theory
2D materials

ABSTRACT

Alkali metal decorated 2D materials represent a promising approach for reversible hydrogen storage, a critical component in the transition to clean energy sources. This study investigates PHE-graphene, comprising 5-, 6- and 9-membered carbon rings, as sodium (Na)-decorated substrate for hydrogen storage applications. The structural, mechanical, and electronic properties of PHE-graphene were analyzed using density functional theory calculations. The lattice decoration with Na was found to promote ideal physical adsorption of H_2 molecules, with adsorption energies ranging from −0.33 to −0.23 eV, achieving a gravimetric hydrogen storage capacity of up to 8.79 wt%, exceeding the U.S. Department of Energy (DOE) target. *Ab initio* molecular dynamics simulations confirmed the thermal stability of the system, while desorption temperature calculations highlighted favorable conditions for reversible H_2 storage. These findings position Na-decorated PHE-graphene as a promising and efficient solution for sustainable hydrogen systems.

1. Introduction

Carbon is a versatile element, capable of forming chemical bonds through different hybridization states (sp, sp^2, and sp^3) [1]. This adaptability enables the formation of a wide range of nanostructures across different dimensions: zero-dimensional (0D) like carbon dots and fullerenes [2], one-dimensional (1D) forms such as carbon nanotubes and nanoribbons [3], two-dimensional (2D) materials including graphene and graphynes [4], and three-dimensional (3D) structures like graphite and diamond [5].

Graphene, in particular, has been extensively studied due to its unique electronic, optical, and mechanical properties [6]. In addition, several 2D carbon allotropes have been proposed, some also exhibiting metallic behavior, such as the biphenylene network (BPN) [7], T-graphene [8], Irida-graphene [9], and DHP-graphene [10]. Others, in contrast, demonstrate semiconducting characteristics, including penta-graphene [11], the monolayer fullerene network (2D-C_{60}) [12], graphenylene [13], and graphenyldiene [14,15]. The discovery and synthesis of new carbon-based materials have often relied on molecular precursors [16–18]. For example, systems such as 2D-C_{60} and biphenylene have been successfully synthesized utilizing the controlled polymerization of small carbon-based molecules [7,12,19,20].

Among the computationally predicted carbon allotropes, the C65 – also known as PHE-graphene – has gained attention due to its structural and electronic properties [21–23]. First proposed in 2013 as C65 by Lu and Li [24], this material features a periodic network where hexagonal (C6) units are interconnected by pentagonal (C5) rings, resulting in a metallic and thermodynamically stable framework. Independently, Zeng et al. [25] later rediscovered the same structure, referring to it as PHE-graphene to emphasize its composition of pentagons (P), hexagons (H), and enneagons (E). Further theoretical investigations suggested that PHE-graphene could enhance the performance of lithium-sulfur (Li–S) batteries by mitigating the polysulfide shuttle effect and improving cathode conductivity [25].

The experimental realization of PHE-graphene remains an open avenue for exploration. Theoretical studies have investigated molecular precursors that could serve as potential building blocks for such structures [26–28]. Acepentalene, a fundamental structural motif in this material, has been proposed as a key component for constructing novel carbon architectures [26]. For instance, acepentalene-based

* Corresponding authors.
E-mail addresses: jose.laranjeira@unesp.br (J.A.S. Laranjeira), xihaochen@cqwu.edu.cn (X. Chen).

https://doi.org/10.1016/j.ijhydene.2025.151442
Received 5 April 2025; Received in revised form 7 August 2025; Accepted 8 September 2025
Available online 23 September 2025

nanostructures have been explored, demonstrating their stability and potential for forming extended 2D networks with tunable electronic and magnetic properties [27,28]. These studies provide valuable insights into chemical routes that could enable the development of complex carbon networks, including structures related to PHE-graphene.

Regarding the various theoretical applications proposed for PHE-graphene, hydrogen (H_2) storage has garnered particular interest. First, Yadav et al. [22] shows a possible design of lithium-decorated PHE-graphene to retain H_2 molecules. Advancing on this matter, the Ca decoration also demonstrated to be capable of inducing a high gravimetric capacity on PHE-graphene, achieving 8.45 wt% [29], superior to the target recommended by the U.S. Department of Energy (DOE) (6.5 wt%)

In this work, we investigate the potential of sodium-decorated PHE-graphene as a hydrogen storage material using density functional theory (DFT) calculations. A detailed analysis of its structural, mechanical, and electronic properties is conducted to evaluate its suitability for metal decoration and hydrogen adsorption. The interaction of H_2 molecules with Na-decorated PHE-graphene is examined, including adsorption energies, charge transfer, hydrogen storage capacity, and desorption dynamics. Additionally, *ab initio* molecular dynamics (AIMD) simulations are performed to assess the thermal stability of the substrate and the feasibility of reversible hydrogen storage. This study aims to provide new insights into the potential of PHE-graphene as an efficient material for sustainable hydrogen storage applications.

2. Methodology

We performed first-principles calculations within the DFT framework to characterize the physicochemical properties of PHE-graphene and evaluate its potential as a hydrogen storage material. These calculations used the generalized gradient approximation (GGA) formulated by Perdew, Burke, and Ernzerhof (PBE) [30,31]. The projector augmented wave (PAW) method [32] was also utilized, and both approaches were implemented within the Vienna *ab initio* Simulation Package (VASP). The electronic wave functions were expanded using a plane-wave basis set with a kinetic energy cut-off of 520 eV. A vacuum spacing of 15 Å was introduced along the z-axis to mitigate interactions between periodic images.

The structural optimization calculations and the projected density of states (PDOS) calculations used Γ-centered **k**-point meshes with grid sizes of $6 \times 6 \times 1$ and $9 \times 9 \times 1$, respectively. Dispersion interactions were considered using the DFT-D2 correction scheme proposed by Grimme [33]. Structural relaxation was performed using the conjugate gradient method, with convergence criteria requiring that total energy variations for the atomic and lattice parameters remain below 1×10^{-5} eV, and the Hellmann–Feynman forces on the individual atoms did not exceed 0.01 eV/Å. *Ab initio* molecular dynamics (AIMD) simulations were used to assess the thermal stability and reversibility of hydrogen storage in sodium functionalized PHE-graphene (Na@PHE-graphene). Furthermore, the Bader charge decomposition method analyzed the charge transfer mechanism.

The adsorption energy (E_{ads}) for Na@PHE-graphene + nH$_2$ systems was computed using the following expression:

$$E_{ads} = \frac{1}{n}\left(E_{Na@PHE\ +\ nH_2} - E_{Na@PHE} - nH_2\right), \quad (1)$$

where $E_{Na@PHE\ +\ nH_2}$ represents the total energy of the Na@PHE-graphene system with n adsorbed H_2 molecules, $E_{Na@PHE}$ is the energy of the bare Na@PHE-graphene substrate, and E_{H_2} corresponds to the energy of an isolated H_2 molecule.

The consecutive adsorption energy (E_{con}) for each additional pair of H_2 molecules adsorbed on the surface was determined as:

$$E_{con} = \frac{1}{2}\left(E_{Na@PHE+nH_2} - E_{Na@PHE+(n-2)H_2} - 2E_{H_2}\right). \quad (2)$$

The hydrogen adsorption capacity (HAC) in weight percentage was calculated as:

$$HAC(wt\%) = \frac{n_H M_H}{n_C M_C + n_{Na} M_{Na} + n_H M_H}, \quad (3)$$

where n_X and M_X represent the number of atoms and molar masses of element X (X = H, C, and Na), respectively.

The hydrogen desorption temperature (T_R) was estimated using the van't Hoff equation [34,35], assuming atmospheric pressure (1 atm):

$$T_{des} = |E_{ads}| \frac{R}{K_B \Delta S}, \quad (4)$$

where R is the universal gas constant, k_B is the Boltzmann constant, and ΔS represents the entropy change associated with the phase transition of hydrogen from the gas phase to the liquid phase (75.44 J mol^{-1} K^{-1}).

A thermodynamic analysis was performed to evaluate the adsorption and desorption behavior of H_2 molecules under realistic conditions, employing the grand canonical partition function Z, given by:

$$Z = 1 + \sum_{i=1}^{n} \exp\left(-\frac{E_i^{ads} - \mu}{k_B T}\right). \quad (5)$$

In this equation, n denotes the total number of H_2 molecules that can be adsorbed, while μ represents the chemical potential of a hydrogen molecule in the gaseous state. Here, E_i^{ads} corresponds to the adsorption energy of the ith H_2 molecule [36,37].

Except for the evaluation of the most stable sites for Na decoration that were performed within a supercell configuration of 2×2, all other calculations presented in this study were performed within the PHE-graphene unit cell. To enhance visualization, periodic images were employed.

3. Results

We begin by presenting a set of structural and electronic properties of the studied material, as shown in Fig. 1. PHE-graphene is characterized by a hexagonal lattice structure within the $P\bar{6}m2$ (No. 187) space group. This lattice features parameters with dimensions $a = b = 5.73$ Å. Within the lattice, there exist three non-equivalent atoms: C_1, located at coordinates (0.0000, 0.0000, 0.0000), C_2 (0.6592, 0.0758, 0.0000), and C_3 (0.1397, 0.8603, 0.0000). The representative cell of PHE-graphene is denoted in Fig. 1a. For a complete assessment of the thermal stability of the monolayer, AIMD simulations were performed with a duration of 5 ps at a temperature of 300 K, where the energy fluctuations are represented in Fig. 1b. The energy oscillations varying around 0.5 eV indicate the stability of the material. Furthermore, there were no detectable structural alterations or deformations, which confirms that the thermal conditions at 300 K do not cause instability in the material.

Fig. 1c presents the band structure of PHE-graphene. This monolayer exhibits metallic characteristics consistent with previously reported findings [25,38]. In the analysis of the PDOS (Fig. 1d), one can observe that the bands are predominantly composed of C(p) states. This observation indicates a pronounced π character in the bonds in PHE-graphene. This trend corroborates the high band dispersion demonstrated by the band structure, which denotes high carrier mobility throughout the Brillouin zone (BZ). The dispersion of the phonon band is analyzed to confirm the dynamic stability of PHE-graphene, as shown in Fig. 1e. It shows a lack of negative phonon modes, as every branch within the entire BZ region presents positive frequencies and no imaginary modes.

The PHE-graphene membrane's mechanical properties were investigated to assess its structural stability and response under mechanical deformation. Our analysis indicates that the monolayer is characterized by three distinct elastic constants: $C_{11} = C_{22} = 281.64$ N/m, $C_{12} = C_{21} = 73.83$ N/m, and $C_{66} = 103.90$ N/m. These values are consistent with the expected symmetry of PHE-graphene, as they satisfy the relation $C_{11} = C_{22}$ and $2 \cdot C_{66} = C_{11} - C_{12}$ [39]. These results highlight the intrinsic

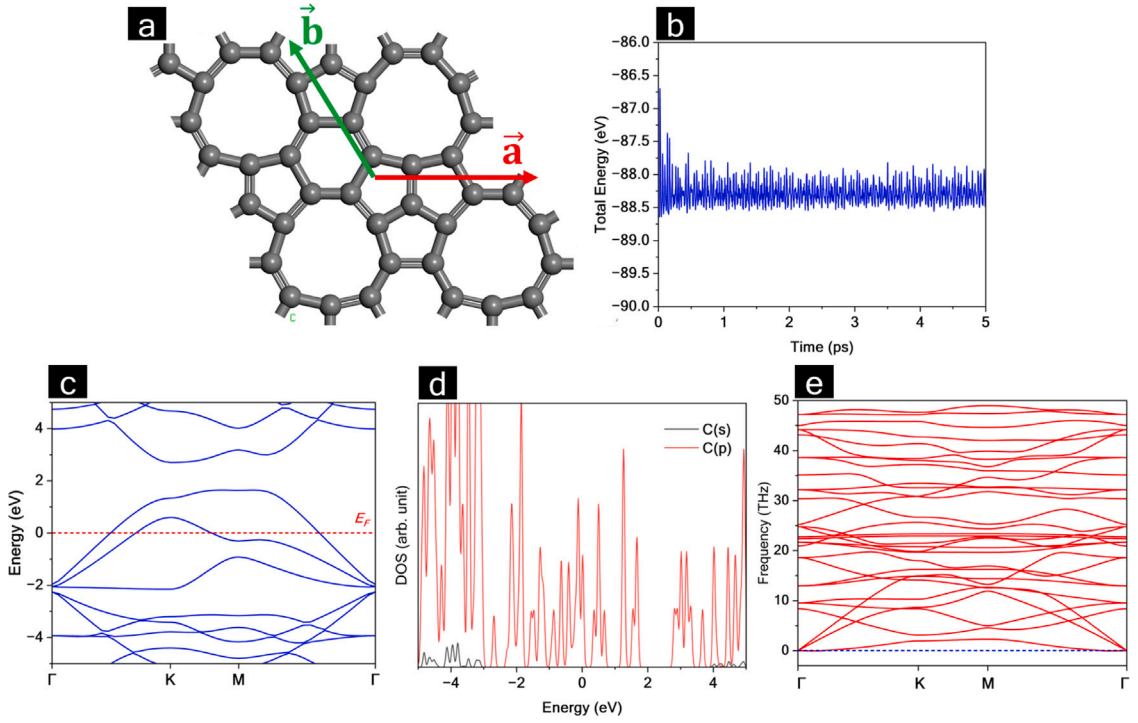

Fig. 1. PHE-graphene monolayer: (a) representative cell, (b) AIMD total energy, (c) band structure, (d) PDOS, and (e) phonon dispersion. The Fermi level (E_F) is set to 0 eV and indicated by the red dashed line in (c).

strength and structural stability of the material. Furthermore, they comply with the Born–Huang stability criteria for hexagonal lattices, which require conditions such as $C_{11} > 0$ and $C_{11} > |C_{12}|$ [40].

This symmetry also ensures the PHE-graphene monolayer exhibits isotropic mechanical behavior. Specifically, it has a Young's modulus of $Y = (C_{11}^2 - C_{22}^2)/C_{11} = 262.3$ N/m, a shear modulus of $G = C_{66} = 103.90$ N/m, and a Poisson's ratio of $\nu = C_{12}/C_{11} = 0.26$, classifying PHE-graphene as a ductile nanomaterial ($\nu > 0.25$) [41]. These results are in agreement with previous findings in the literature [21].

To examine the Na decoration in the PHE-graphene monolayer, we considered nine high-symmetry sites, depicted in Fig. 2. These included three pore sites (P1, P2, and P3), three atomic sites (A1, A2, and A3), and two bridge sites (B1, B2, and B3), to determine the most stable adsorption configuration for the Na adatom. Table 1 presents the adsorption energies (E_{ads}) and the final optimized sites. The findings indicate that the P3 site is the most stable site for Na adsorption, demonstrating a E_{ads} of −2.57 eV. This value is higher than (in the module) the cohesive energy of the Na bulk (−1.05 eV/atom) [42], and comparable to that observed for Ca-decorated PHE-graphene (E_{ads} = −3.23 eV). In addition, elevated E_{ads} values were observed for sites A1 (−2.17 eV) and P1 (−2.24 eV). These observations suggest that the Na adsorption on PHE-graphene inhibits any tendency for clusterization and can be stable around all available surface sites.

Following the previous results, the Na loading was carried out at the P3 site of the PHE-graphene membrane, with Na adatoms placed up and down the monolayer plane. Subsequently, thermal stability of Na@PHE-graphene was examined using AIMD simulations, as represented in Fig. 3. At the end of the calculation, it is confirmed that the Na adatoms persist in their most stable locations, specifically the P3 site. The PHE-graphene monolayer also maintains its structural integrity without showing significant changes. These observations highlight the robustness of Na@PHE-graphene as a substrate suitable for hydrogen storage applications since the Na adatom is still retained in the monolayer, preventing metal movement toward the material.

The surface mobility of adsorbed sodium atoms can lead to clustering, thereby reducing the number of active sites available for hydrogen adsorption. To assess the likelihood of such diffusion processes, we employed the nudged elastic band (NEB) method [43–45], as illustrated

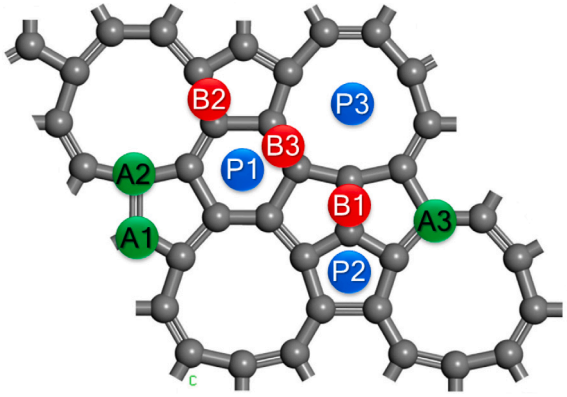

Fig. 2. The high-symmetry sites explored for the Na decoration on PHE-graphene.

Table 1
Adsorption energies (E_{ads}) and final configurations of Na adsorption sites on PHE-graphene.

Initial site	E_{ads} (eV)	Final site
A1	−2.17	A1
A2	−2.17	A1
A3	−2.17	A1
B1	−2.17	A1
B2	−2.17	A1
B3	−2.24	P1
P1	−2.24	P1
P2	−2.17	A1
P3	−2.57	P3

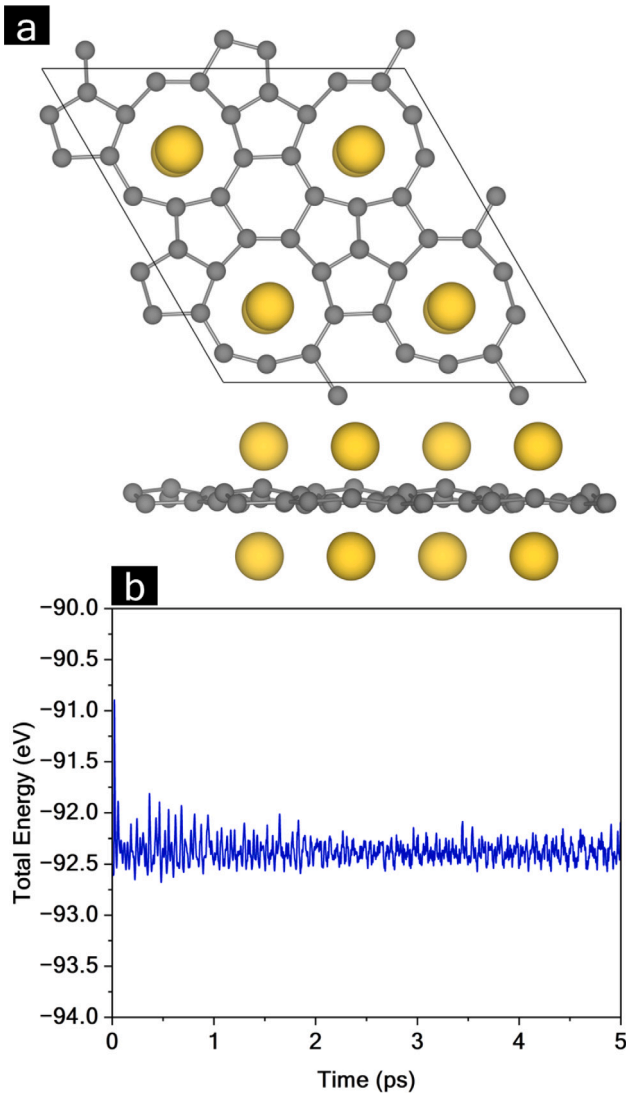

Fig. 3. (a) Optimized structure and (b) total energy profile from AIMD simulation of the Na@PHE-graphene system.

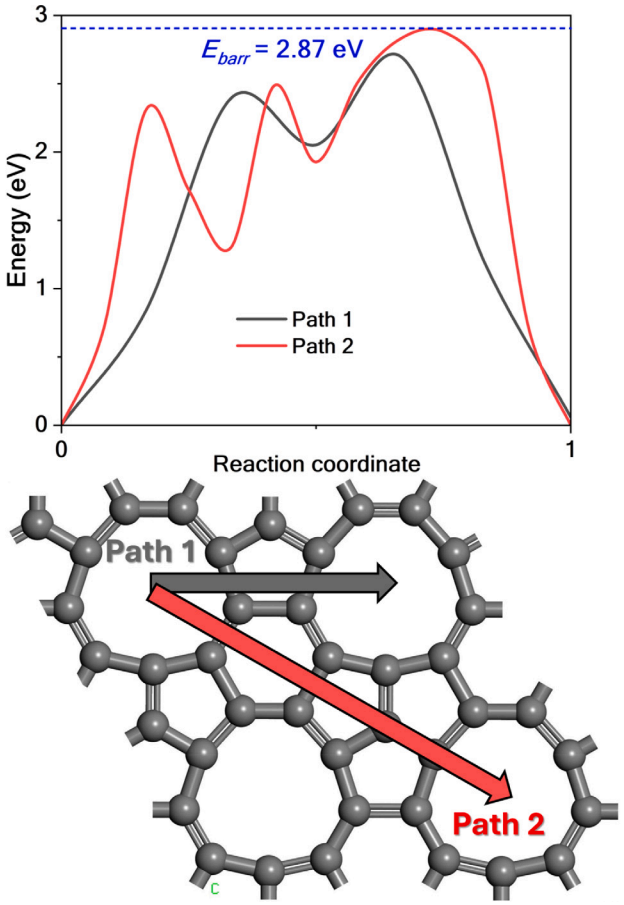

Fig. 4. Diffusion energy profile for a Na atom migrating along Path 1 (gray) and Path 2 (red). The diffusion energy barrier is calculated to be 2.87 eV. (For interpretation of the references to color in this figure legend, the reader is referred to the web version of this article.)

in Fig. 4. Two distinct diffusion pathways were considered. The calculated diffusion barrier for sodium migration was approximately 2.87 eV, indicating a very low probability of spontaneous diffusion under ambient conditions. This barrier is significantly higher than the thermal energy available to a single atom at room temperature (300 K), which can be estimated using the classical expression:

$$E_{\text{thermal}} = \frac{3}{2} k_B T \tag{6}$$

where $k_B = 8.617 \times 10^{-5}$ eV/K is the Boltzmann constant. Substituting the temperature:

$$E_{\text{thermal}} = \frac{3}{2} \times 8.617 \times 10^{-5} \times 300 \approx 0.039\,\text{eV}. \tag{7}$$

Thus, the diffusion barrier of 2.87 eV is significantly greater than the thermal energy at 300 K, confirming that spontaneous migration of Na atoms is thermally inaccessible under standard conditions and would require elevated temperatures or external activation to occur.

The electronic structure of Na@PHE-graphene was investigated using the band structure and PDOS, as illustrated in Fig. 5. One can note that Na@PHE-graphene maintains the metallic behavior exhibited by the pristine monolayer. However, it can be verified that the Fermi energy (E_F) (which is represented by 0 eV in the Figure, but its real value is −0.50 eV) is found in an elevated position concerning the observed condition for the pure monolayer (−3.59 eV). As supported by the PDOS data, these bands are also composed of Na states. This trend indicates that the Na atoms act as electron donors, making the unoccupied levels now occupied. For the valence band (VB), there are no significant changes in the band dispersion. However, for the conduction band (CB), the emergence of several new bands is notable. As seen in PDOS, these bands possess a higher contribution of Na(s) states, with levels immediately after E_F composed of these states. Within the range examined, it is evident that the C(p) states predominantly govern the overall distribution. For Na adatoms, the primary contributions come from the Na(s) states. Furthermore, it is evident that there is a coupling between the C(p) and Na(s) states around the E_F and the interaction between Na and PHE-graphene. The electronic role mentioned of sodium in this system is desirable for further H_2 adsorption, as the metal can act by modulating the charge transfer between hydrogen and the PHE-graphene substrate.

Fig. 6 shows the charge density difference (CDD) map for the Na@PHE-graphene system. It is observable that the regions where the charge is depleted are situated within the plane of the monolayer, whereas the areas where the charge accumulates are above this plane. This observation is consistent with the previous PDOS analysis, indicating that the π states of the monolayer actively engage in interactions with the Na adatoms. Furthermore, a Bader charge analysis revealed a charge transfer of 0.73 $|e|$/Na from the Na adatoms to the monolayer.

H_2 saturation was carried out on the Na@PHE-graphene substrate, as depicted in Fig. 7. The adsorption energy (E_{ads}), HAC, consecutive

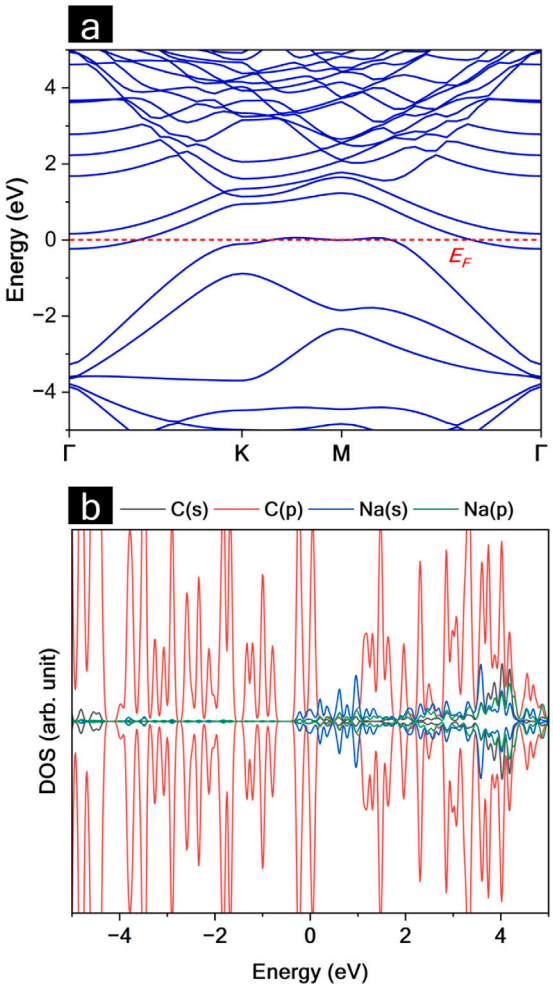

Fig. 5. (a) Electronic band structure and (b) PDOS of the Na@PHE-graphene system. The Fermi level (E_F) is set to 0 eV and indicated by the red dashed line.

adsorption energy ($\mathbf{E_{con}}$), average H–H bond length ($R_{H\text{-}H}$), and desorption temperature (T_{des}) for each configuration are summarized in Table 2 and Fig. 8. The calculated E_{ads} values range from −0.33 to −0.23 eV, indicating a physisorption-dominated interaction essential to achieve reversible hydrogen storage [46]. As observed in H_2 adsorption studies on other 2D-based materials [47–49], the sequential introduction of hydrogen molecules results in a progressive reduction of adsorption energy, primarily due to steric effects. Furthermore, since Na decoration modulates charge transfer, the electrostatic contribution further reduces the magnitude of E_{ads}, strengthening the influence of charge redistribution on the adsorption mechanism.

The E_{con} was further analyzed to determine whether adding more H_2 molecules onto Na@PHE-graphene is energetically favorable. If $E_{con} < 0$, the additional $2H_2$ molecules are energetically favored for adsorption and remain attracted to the substrate. Conversely, if $E_{con} > 0$, the added $2H_2$ molecules tend to stay free, indicating a preference not to adhere to the substrate.

Analysis revealed that Na@PHE-graphene + $8H_2$ exhibited the highest E_{con} value (−0.23 eV), while Na@PHE-graphene + $2H_2$ displayed the lowest value (−0.66 eV). These findings indicate that additional H_2 molecules do not introduce instability into the system. Regarding HAC, Na@PHE-graphene achieves a maximum storage capacity of 8.79 wt% with $8H_2$ molecules, reinforcing its potential as a highly promising substrate for H_2 storage.

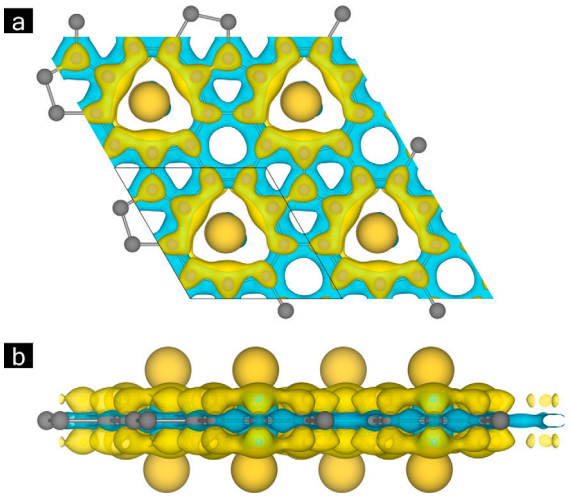

Fig. 6. Charge density difference map for the Na@PHE-graphene system, shown from (a) top and (b) side views, where yellow and blue represent charge accumulation and depletion, respectively. (For interpretation of the references to color in this figure legend, the reader is referred to the web version of this article.)

Table 2
Adsorption energy (E_{ads}), hydrogen adsorption capacity (HAC), consecutive adsorption energy (E_{con}) average H–H bond length ($R_{H\text{-}H}$), and desorption temperature (T_{des}) for Na@PHE-graphene + nH_2 (n = 2, 4, 6, 8).

System	E_{ads} (eV)	E_{con} (eV)	HAC (wt%)	$R_{H\text{-}H}$ (Å)	T_{des} (K)
Na@PHE-graphene + $2H_2$	−0.33	−0.33	2.35	0.76	423
Na@PHE-graphene + $4H_2$	−0.28	−0.24	4.60	0.77	363
Na@PHE-graphene + $6H_2$	−0.27	−0.23	6.74	0.77	339
Na@PHE-graphene + $8H_2$	−0.23	−0.11	8.79	0.76	290

Importantly, average H–H bond length ($R_{H\text{-}H}$) remains nearly constant regardless of the increasing number of adsorbed H_2 molecules. This consistency suggests that adsorption does not alter the structural integrity of the H_2 molecules, further confirming the physical nature of the interaction. Examining the desorption temperature (T_{des}) indicates that relatively moderate temperatures are required for H_2 release, ranging from 290 K (Na@PHE-graphene + $8H_2$) to 423 K (Na@PHE-graphene + $2H_2$). These desorption temperatures highlight the favorable thermodynamics and kinetics of reversible hydrogen storage on the Na@PHE-graphene substrate.

The hydrogen storage performance of the Na@PHE-graphene system was analyzed and compared with other systems reported in the literature, as summarized in Table 3. This comparison considers key parameters, including the total number of adsorbed H_2 molecules (n), the absolute adsorption energy per H_2 ($|E_{ads}|$), HAC, and T_{des}.

One can note that Na@PHE-graphene system can hold up to 8 H_2 molecules, with an adsorption energy of 0.23 eV per H_2. This value of E_{ads} is higher, in magnitude, than those observed in other Na-decorated systems like Na@B_7N_5 ($|E_{ads}|$ = 0.20 eV) [47], Na@Irida-G ($|E_{ads}|$ = 0.14 eV) [50], and Na@IGP-SiC ($|E_{ads}|$ = 0.10 eV) [48], as well as in other alkali-based systems such as Li@α-C_3N_2 ($|E_{ads}|$ = 0.22 eV) [51], Li@B_5N_3 ($|E_{ads}|$ = 0.21 eV) [52] and Sc@Ψ-graphene ($|E_{ads}|$ = 0.16 eV) [53], demonstrating the enhanced hydrogen affinity of Na@PHE-graphene. It is evident that the hydrogen adsorption capacity measured for Na@PHE-graphene, which is 8.79 wt%, significantly exceeds that of several systems presented in Table 3, including Na@B_7N5 (7.70 wt%), Li@IGP-SiC (8.27 wt%), Li@irida-graphene (7.06 wt%), and V@biphenylene (7.52 wt%). However, it is still lower than the 14.08 wt% capacity found in Li@β12-borophene/graphene bilayer.

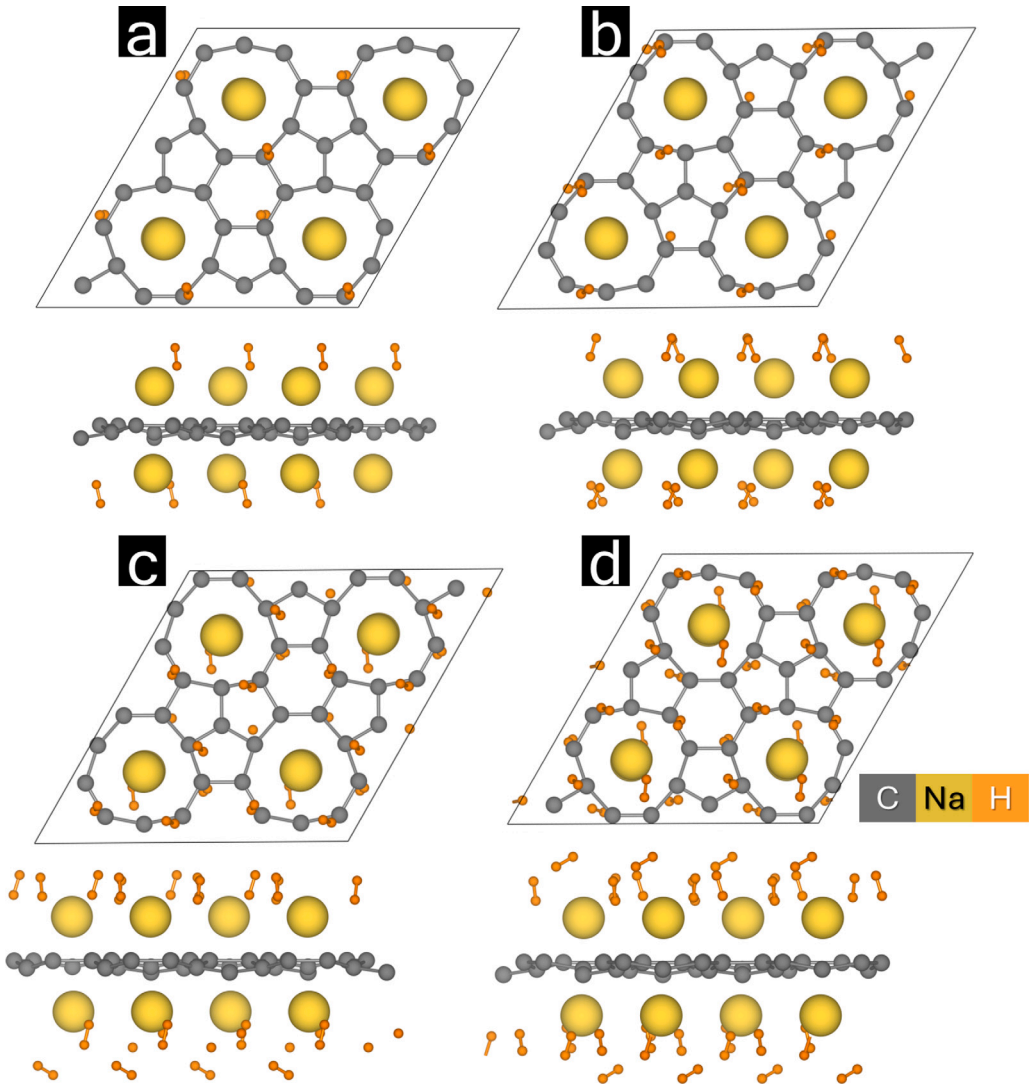

Fig. 7. Stepwise approach to achieving maximum H_2 saturation on Na@PHE-graphene, where (a), (b), (c), and (d) correspond to the system with 2, 4, 6, and 8 H_2 molecules, respectively. The stoichiometry reflects the H_2 molecules per PHE-graphene unit cell.

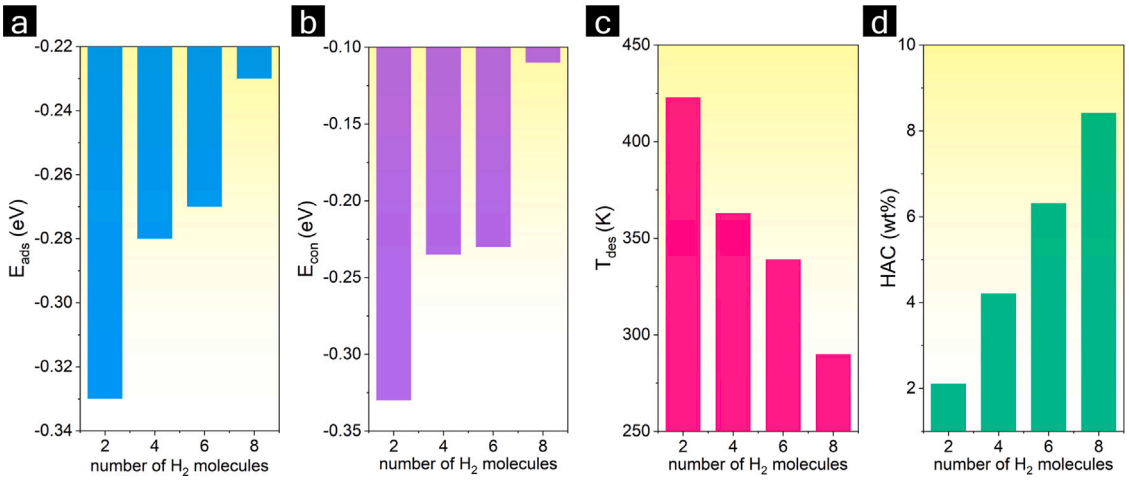

Fig. 8. (a) Adsorption energy (E_{ads}), (b) consecutive adsorption energy (E_{con}), (c) desorption temperature (T_{des}), and (d) HAC for Na@PHE-graphene + nH_2 (n = 2, 4, 6, 8).

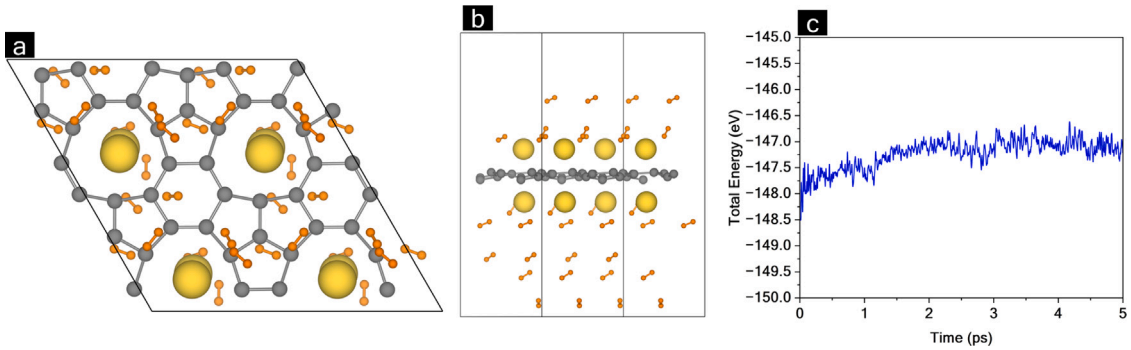

Fig. 9. Final structure of the Na@PHE-graphene + 8H_2 system shown from (a) top and (b) side views, along with (c) the energetic profile from AIMD simulation at 300 K.

Table 3
Total number of adsorbed H_2 molecules (n), Absolute adsorption energy per H_2 ($|E_{ads}|$), Hydrogen Adsorption Capacity (HAC), and Desorption temperature (T_{des}) associated with configurations exhibiting complete H_2 coverage configurations in recently documented systems.

System	n	$\|E_{ads}\|$ (eV)	HAC (wt%)	T_{des} (K)
Na@PHE-graphene (this work)	8	0.23	8.79	290
K@PHE-graphene [54]	32	0.33	7.47	422
Na@B_7N_5 [47]	32	0.20	7.70	257
Na@Irida-graphene [50]	32	0.14	7.82	195
Na@DHP-graphene [55]	12	0.14	11.21	–
Na@IGP-SiC [48]	48	0.10	6.78	148
Li@IGP-SiC [48]	48	0.14	8.27	191
Li@B_5N_3 [52]	13	0.21	6.30	267
Li@net-Y [56]	24	0.27	9.0	348
Li@α-C_3N_2 [51]	12	0.22	5.7	285
Li@POG-$B_4C_2N_3$ [57]	10	0.19	8.35	245
Li@β_{12}-borophene [58]	4	0.10	11.59	–
V@Biphenylene [59]	5	0.51	7.52	596
Ca@PHE-graphene [29]	24	–	8.45	–
Sc@Ψ-graphene [53]	9	0.16	14.46	203

Regarding desorption temperature, the Na@PHE-graphene system demonstrates a moderate value of 290 K, which is lower than those observed in systems like Li@net-Y (348 K) and Li@irida-graphene (353 K) but similar to Li@α-C_3N_2 (285 K) and Li@B14 (271 K). This desorption temperature suggests that Na@PHE-graphene is well-suited for hydrogen storage applications requiring moderate thermal conditions for hydrogen release. Additionally, we can observe a strong correlation between adsorption energy and desorption temperature. The V@biphenylene complex shows a higher T_{des} (0.51 eV) due to stronger H_2 adsorption, significantly exceeding the value for Na@PHE-graphene, where the hydrogen-substrate interaction is more balanced. Most notably, we compared our H_2 storage results with those reported for K-decorated PHE-graphene. While the K-functionalized system exhibited a lower storage capacity of 7.47 wt%, our Na-decorated structure not only demonstrated higher uptake but also offered improved desorption kinetics and greater reversibility. This enhanced performance is attributed to the more favorable adsorption energy range of Na (from −0.33 to −0.23 eV/H_2), which is significantly less negative than the values reported for K (from −2.59 to −0.33 eV/H_2), suggesting weaker binding and thus more facile release of hydrogen in the Na system.

AIMD simulations were performed at 300 K for 5 ps, as shown in Fig. 9, which provides top and side views of the final structure along with the corresponding energy fluctuations. The results reveal that the Na adatoms remain stable in their positions after the simulation, indicating that the configuration is stable even in the absence of H_2 molecules. This feature suggests that H_2 adsorption does not destabilize the Na@PHE-graphene substrate. Furthermore, our results are consistent with the previously obtained T_{des} data, showing that most

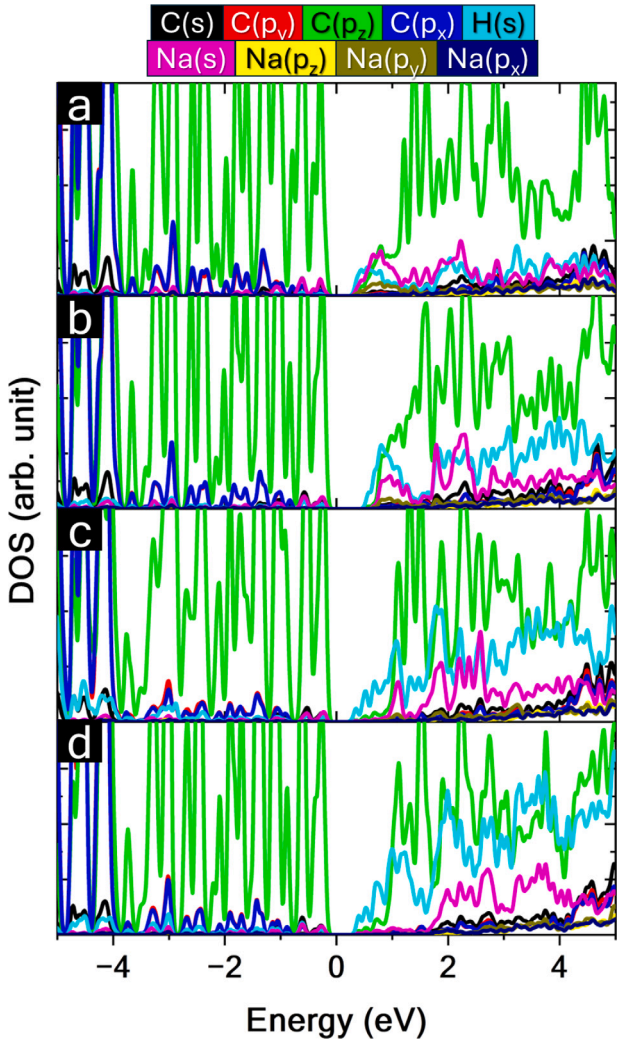

Fig. 10. PDOS for (a) Na@PHE-graphene + 2H_2, (b) Na@PHE-graphene + 4H_2, (c) Na@PHE-graphene + 6H_2, and (d) Na@PHE-graphene + 8H_2. The Fermi energy was set to 0 eV.

H_2 molecules desorb at 300 K, highlighting the rapid kinetics of desorption. Energy fluctuations further confirm that after 2 ps, significant changes cease, supporting the stability of the final configuration at 300 K.

To investigate changes in the electronic structure induced by H_2 adsorption, we calculated the PDOS for the Na@PHE-graphene + $n$$H_2$

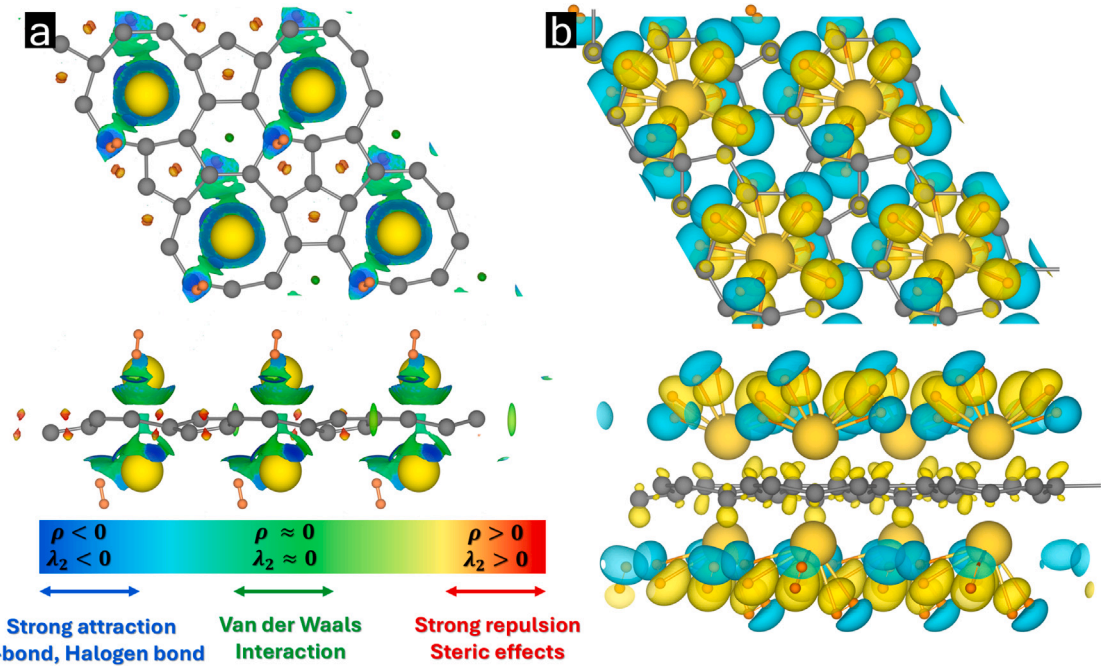

Fig. 11. (a) Side and top views of the reduced density gradient (RDG), highlighting the nature and strength of intermolecular interactions in the Na@PHE-graphene + $2H_2$ system. (b) Charge density difference map of Na@PHE-graphene + $8H_2$ shown from top and side views, where yellow and blue represent charge accumulation and depletion, respectively. (For interpretation of the references to color in this figure legend, the reader is referred to the web version of this article.)

($n = 2, 4, 6, 8$) configurations, as illustrated in Fig. 10. The VB was dominated by the C(p) states, with the distribution of electronic levels not significantly altered by H_2 adsorption. At the CBM, the H(s) states show a more significant contribution. For higher energy levels in CB, the coupling between C(p), H(s), and Na(s, and p) is elevated. Specifically, the appearance of a band gap energy is noticeable, with values of 0.44 eV ($2H_2$), 0.72 eV ($4H_2$), 0.06 eV ($6H_2$), and 0.50 eV ($8H_2$). These findings highlight the ability of Na@PHE-graphene to serve as a substrate for potential applications in H_2 sensor-based devices.

Now, we discuss the electronic modifications induced by the introduction of hydrogen molecules. To this end, the charge density difference (CDD), and reduced density gradient (RDG) maps are presented in Fig. 11. The RDG map was calculated for Na@PHE-graphene + $2H_2$, as denoted in Fig. 11a. It can be noticed that the interaction between the H_2 molecules and the substrate lies between strong attraction and van der Waals interaction. This aligns with the adsorption energies measured, which fall below −0.1 eV/H_2, ruling out pure physisorption, and are substantially higher than −0.6 eV/H_2, also ruling out chemisorption. Thus, we can classify the interaction between the H_2 and substrate as a reversible chemisorption.

The CDD map, as shown in Fig. 11b, was employed to investigate the dynamics of charge redistribution. The CDD map reveals simultaneous zones of charge accumulation (yellow) and depletion (blue) for H_2 molecules, indicating polarization. Moreover, regions where small charges accumulate have been observed in PHE-graphene. This observation suggests that when Na@PHE-graphene interacts, it acquires a certain amount of charge. This charge transfer results in an upward shift of the Fermi level (E_F) of 1.06 eV (the E_F value for Na@PHE-graphene + $8H_2$ system is equal to 0.56 eV), leading to a transition of the material to a semiconductor state. The Bader charge analysis reinforces these findings by demonstrating that the monolayer charge amounts to $-1.46|e|$. This value is higher in magnitude than that observed for Na@PHE-graphene case. Specifically, the charge associated with Na adatoms is $+0.82|e|$/Na, while the charge exhibited by the H_2 molecules is $-0.08\ |e|/H_2$.

The minimally significant charge of the H_2 molecules aligns with the physical adsorption, as indicated by the E_{ads} values. These results highlight the influence of Na adatoms in facilitating the H_2 molecule retention under a reversible regime on the substrate.

Finally, Fig. 12 presents an analysis of the thermodynamics concerning the number of H_2 molecules influenced by temperature (T) and pressure (P). To evaluate the practical applicability of our material in light of DOE hydrogen storage targets [60], we assessed the number of H_2 molecules adsorbed under the prescribed pressure (5–12 bar) and temperature (−40 to 85 °C) windows. Our results indicate that at the lower temperature bound (−40 °C), the material retains a high storage capacity, adsorbing 6.37 H_2 (HAC = 7.12 wt%) molecules at 5.15 atm and 6.53 H_2 (HAC = 7.29 wt%) molecules at 11.97 atm. However, at the upper temperature limit (85 °C), the number of adsorbed H_2 molecules drops to 0.02 for both 5.15 and 11.97 atm. These values are consistent with the expected thermodynamic behavior, as higher temperatures promote desorption. Importantly, the high uptake at low temperature and relevant pressures demonstrates that the material satisfies the DOE's storage window during hydrogen filling, while the rapid release at elevated temperatures enables efficient hydrogen delivery, as required for onboard applications. These results underscore that Na@PHE-graphene presents an effective hydrogen storage solution under realistic temperature and pressure conditions.

4. Conclusions

In this work, we investigate the hydrogen storage potential of sodium-decorated PHE-graphene using DFT. The structural, mechanical, and electronic properties and interaction with H_2 molecules are thoroughly analyzed. PHE-graphene demonstrates significant structural stability, as confirmed by phonon dispersion analysis and AIMD simulations at 300 K. The material exhibits remarkable mechanical robustness, with a Young's modulus of 281.64 N/m and a shear modulus of 103.90 N/m, ensuring its integrity under functionalization. Electronically, sodium-decorated PHE-graphene retains metallic characteristics with pronounced band dispersion near the Fermi level. Functionalization with sodium improves the adsorption energy, ranging from −0.33 to −0.23 eV, enabling a gravimetric storage capacity of up to

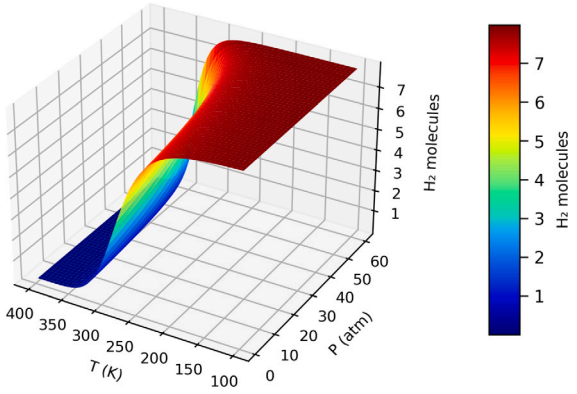

Fig. 12. The average number of adsorbed H_2 on Na@PHE-graphene at various temperatures (T) and pressures (P).

8.79 wt%, surpassing the DOE target. Desorption temperature calculations reveal favorable conditions for reversible hydrogen storage with rapid desorption kinetics under ambient conditions. Na@PHE-graphene demonstrated semiconductor-like properties when exposed to H_2 adsorption, with a band gap of 0.50 eV. This observation suggests the potential of the substrate as an alternative solution for hydrogen storage and in the detection of H_2 molecules. These findings position PHE-graphene as a promising and efficient candidate for sustainable hydrogen storage applications.

CRediT authorship contribution statement

José A.S. Laranjeira: Writing – review & editing, Writing – original draft, Validation, Methodology, Investigation, Formal analysis, Data curation, Conceptualization. **Nicolas F. Martins:** Writing – review & editing, Writing – original draft, Validation, Formal analysis, Data curation. **Kleuton A.L. Lima:** Writing – review & editing, Validation, Data curation. **Luiz A. Ribeiro:** Writing – review & editing, Visualization, Formal analysis, Data curation. **Marcelo L. Pereira:** Writing – review & editing, Writing – original draft, Visualization, Validation, Formal analysis, Data curation. **Julio R. Sambrano:** Writing – review & editing, Visualization, Resources. **Xihao Chen:** Writing – review & editing, Writing – original draft, Visualization, Supervision, Investigation, Formal analysis, Conceptualization.

Declaration of competing interest

The authors declare that they have no known competing financial interests or personal relationships that could have appeared to influence the work reported in this paper.

Acknowledgments

X.C. was funded by the Research Program of the Chongqing Municipal Education Commission (Grants No. KJQN202201327 and KJQN202301339). This work was supported by the Brazilian funding agencies: the São Paulo Research Foundation (FAPESP, Grants No. 2022/03959-6, 2024/05087-1, 2020/01144-0, and 2022/16509-9) and the National Council for Scientific and Technological Development (CNPq, Grant No. 307213/2021–8). M.L.P.J. acknowledges financial support from the Research Support Foundation of the Federal District (FAP-DF, Grant No. 00193-00001807/2023-16) and CNPq (Grant No. 444921/2024-9). L.A.R.J. acknowledges the financial support from FAP-DF grants 00193.00001808/2022-71 and 00193-00001857/2023-95, FAPDF-PRONEM grant 00193.00001247/2021-20, PDPG-FAPDF-CAPES Centro-Oeste 00193-00000867/2024-94, and CNPq grants 350176/2022-1 and 167745/2023-9.

Data access statement

Data supporting the results can be accessed by contacting the corresponding author.

References

[1] Hajialilou Ehsan, Rezanezhad Armin, Hanif Muhammad Bilal, Motola Martin. Two-dimensional carbon graphenylene. In: Handbook of functionalized carbon nanostructures: from synthesis methods to applications. Springer; 2023, p. 1–37.
[2] Breczko Joanna, Wysocka-Żołopa Monika, Grądzka Emilia, Winkler Krzysztof. Zero-dimensional carbon nanomaterials for electrochemical energy storage. ChemElectroChem 2024;e202300752.
[3] Allard Charlotte, Alvarez Laurent, Bantignies Jean-Louis, Bendiab Nedjma, Cambré Sofie, Campidelli Stephane, Fagan Jeffrey A, Flahaut Emmanuel, Flavel Benjamin, Fossard Frédéric, et al. Advanced 1D heterostructures based on nanotube templates and molecules. Chem Soc Rev 2024.
[4] Zheng Jia-Jia, Zhao Xiang, Zhao Yuliang, Gao Xingfa. Two-dimensional carbon compounds derived from graphyne with chemical properties superior to those of graphene. Sci Rep 2013;3(1):1271.
[5] Bianco Alberto, Chen Yongsheng, Chen Yuan, Ghoshal Debjit, Hurt Robert H, Kim Yoong Ahm, Koratkar Nikhil, Meunier Vincent, Terrones Mauricio. A carbon science perspective in 2018: Current achievements and future challenges. Carbon 2018;132:785–801.
[6] Singh Virendra, Joung Daeha, Zhai Lei, Das Soumen, Khondaker Saiful I, Seal Sudipta. Graphene based materials: past, present and future. Prog Mater Sci 2011;56(8):1178–271.
[7] Fan Qitang, Yan Linghao, Tripp Matthias W, Krejčí Ondřej, Dimosthenous Stavrina, Kachel Stefan R, Chen Mengyi, Foster Adam S, Koert Ulrich, Liljeroth Peter, et al. Biphenylene network: A nonbenzenoid carbon allotrope. Science 2021;372(6544):852–6.
[8] De Vasconcelos Fabrício Morais, Souza Filho Antônio Gomes, Meunier Vincent, Girão Eduardo Costa. Electronic properties of tetragraphene nanoribbons. Phys Rev Mater 2019;3(6):066002.
[9] Júnior M L Pereira, da Cunha Wiliam Ferreira, Giozza William Ferreira, de Sousa Junior Rafael Timoteo, Junior LA Ribeiro. Irida-graphene: A new 2D carbon allotrope. FlatChem 2023;37:100469.
[10] Cai Yingxiang, Guo Yuqing, Jiang Bo, Lv Yanan. Encapsulation of cathode in lithium-sulfur batteries with a novel two-dimensional carbon allotrope: DHP-graphene. Sci Rep 2017;7(1):14948.
[11] Zhang Shunhong, Zhou Jian, Wang Qian, Chen Xiaoshuang, Kawazoe Yoshiyuki, Jena Puru. Penta-graphene: A new carbon allotrope. Proc Natl Acad Sci 2015;112(8):2372–7.
[12] Hou Lingxiang, Cui Xueping, Guan Bo, Wang Shaozhi, Li Ruian, Liu Yunqi, Zhu Daoben, Zheng Jian. Synthesis of a monolayer fullerene network. Nature 2022;606(7914):507–10.
[13] Yu Yang-Xin. Graphenylene: a promising anode material for lithium-ion batteries with high mobility and storage. J Mater Chem A 2013;1(43):13559–66.
[14] Laranjeira José AS, Martins Nicolas F, Denis Pablo A, Sambrano Julio R. Graphenyldiene: A new sp2-graphene-like nanosheet. Carbon Trends 2024;14:100321.
[15] Richter Moses, Heumüller Thomas, Matt Gebhard J, Heiss Wolfgang, Brabec Christoph J. Carbon photodetectors: the versatility of carbon allotropes. Adv Energy Mater 2017;7(10):1601574.
[16] Hoheisel Tobias N, Schrettl Stephen, Szilluweit Ruth, Frauenrath Holger. Nanostructured carbonaceous materials from molecular precursors. Angew Chem Int Ed 2010;49(37):6496–515.
[17] Kumar Rajesh, Joanni Ednan, Singh Rajesh K, Singh Dinesh P, Moshkalev Stanislav A. Recent advances in the synthesis and modification of carbon-based 2D materials for application in energy conversion and storage. Prog Energy Combust Sci 2018;67:115–57.
[18] Flores-Lasluisa Jhony Xavier, Navlani-García Miriam, Berenguer-Murcia Ángel, Morallón Emilia, Cazorla-Amorós Diego. 10 years of frontiers in carbon-based materials: carbon, the "newest and oldest" material. The story so far. Front Mater 2024;11:1381363.
[19] Berber Savas, Osawa Eiji, Tománek David. Rigid crystalline phases of polymerized fullerenes. Phys Rev B 2004;70(8):085417.
[20] Hudspeth Mathew A, Whitman Brandon W, Barone Veronica, Peralta Juan E. Electronic properties of the biphenylene sheet and its one-dimensional derivatives. ACS Nano 2010;4(8):4565–70.
[21] Sun Hao, Mukherjee Sankha, Daly Matthew, Krishnan Ajay, Karigerasi Manohar Harsha, Singh Chandra Veer. New insights into the structure-nonlinear mechanical property relations for graphene allotropes. Carbon 2016;110:443–57.
[22] Yadav Shwetank, Tam Jasmine, Singh Chandra Veer. A first principles study of hydrogen storage on lithium decorated two dimensional carbon allotropes. Int J Hydrog Energy 2015;40(18):6128–36.

[23] Jiang Yongzhen, Zou Wenxu, Li Yadong, Cai Yingxiang. Theoretical insights into TM@ PHEs as single-atom catalysts for water splitting based on density functional theory. Phys Chem Chem Phys 2022;24(2):975–81.
[24] Lu Haigang, Li Si-Dian. Two-dimensional carbon allotropes from graphene to graphyne. J Mater Chem C 2013;1(23):3677–80.
[25] Zeng Li, Cai Yingxiang, Xiang Zhihao, Zhang Yu, Xu Xuechun. A new metallic π-conjugated carbon sheet used for the cathode of Li–S batteries. RSC Adv 2019;9(1):92–8.
[26] Zeng Tiantian, Yang Hao, Wang Hongbo, Chen Gang. Acepentalene membrane sheet: a metallic two-dimensional carbon allotrope with high carrier mobility for lithium ion battery anodes. J Phys Chem C 2020;124(11):5999–6011.
[27] Macêdo Luís Eduardo Leite, Kleger Aaron, Meunier Vincent, Girão Eduardo Costa. Electronic properties of carbon sheets and nanoribbons based on acepentalene-like building blocks. Comput Mater Sci 2022;211:111520.
[28] Silva Paloma Vieira, Fadel Mayada, Souza Filho Antonio Gomes, Meunier Vincent, Girao Eduardo Costa. Tripentaphenes: two-dimensional acepentalene-based nanocarbon allotropes. Phys Chem Chem Phys 2020;22(40):23195–206.
[29] Pan Rui, Fan Xiaoli, Luo Zhifen, An Yurong. Calcium decorated two dimensional carbon allotropes for hydrogen storage: A first-principles study. Comput Mater Sci 2016;124:106–13.
[30] Perdew John P, Burke Kieron, Ernzerhof Matthias. Generalized gradient approximation made simple. Phys Rev Lett 1996;77:3865–8, URL https://link.aps.org/doi/10.1103/PhysRevLett.77.3865.
[31] Ernzerhof Matthias, Scuseria Gustavo E. Assessment of the Perdew–Burke–Ernzerhof exchange-correlation functional. J Chem Phys 1999;110(11):5029–36.
[32] Blöchl PE. Projector augmented-wave method. Phys Rev B 1994;50:17953–79, URL https://link.aps.org/doi/10.1103/PhysRevB.50.17953.
[33] Grimme Stefan. Semiempirical GGA-type density functional constructed with a long-range dispersion correction. J Comput Chem 2006;27(15):1787–99.
[34] Durbin Deborah J, Malardier-Jugroot Cecile. Review of hydrogen storage techniques for on board vehicle applications. Int J Hydrog Energy 2013;38(34):14595–617.
[35] Alhameedi Khidhir, Karton Amir, Jayatilaka Dylan, Hussain Tanveer. Metal functionalized inorganic nano-sheets as promising materials for clean energy storage. Appl Surf Sci 2019;471:887–92.
[36] Hashmi Arqum, Farooq M Umar, Khan Imran, Son Jicheol, Hong Jisang. Ultrahigh capacity hydrogen storage in a li decorated two-dimensional C 2 N layer. J Mater Chem A 2017;5(6):2821–8.
[37] Kaewmaraya T, Thatsami N, Tangpakonsab P, Kinkla R, Kotmool K, Menendez C, Aguey-Zinsou KF, Hussain T. Ultrahigh hydrogen storage using metal-decorated defected biphenylene. Appl Surf Sci 2023;629:157391.
[38] Jiang Yongzhen, Zou Wenxu, Li Yadong, Cai Yingxiang. Theoretical insights into TM@PHEs as single-atom catalysts for water splitting based on density functional theory. Phys Chem Chem Phys 2022;24:975–81.
[39] Cadelano Emiliano, Palla Pier Luca, Giordano Stefano, Colombo Luciano. Elastic properties of hydrogenated graphene. Phys Rev B—Condensed Matter Mater Phys 2010;82(23):235414.
[40] Born Max. On the stability of crystal lattices. I. In: Mathematical proceedings of the cambridge philosophical society. Vol. 36, Cambridge University Press; 1940, p. 160–72.
[41] Wang Xiao, Chen Li, Yuan Zhentao, Rong Ju, Feng Jing, Muzammil Iqbal, Yu Xiaohua, Zhang Yannan, Zhan Zhaolin. DHQ-graphene: a novel two-dimensional defective graphene for corrosion-resistant coating. J Mater Chem A 2019;7(15):8967–74.
[42] Jiang Minming, Xu Jiang, Munroe Paul, Xie Zong-Han, Chen Zhaofeng. Light metal decorated graphene-like Si2BN monolayers as hydrogen storage media: A DFT investigation. Int J Hydrog Energy 2024;50:865–78, URL https://www.sciencedirect.com/science/article/pii/S0360319923041757.
[43] Makri Stela, Ortner Christoph, Kermode James R. A preconditioning scheme for minimum energy path finding methods. J Chem Phys 2019;150(9):094109.
[44] Barzilai Jonathan, Borwein Jonathan M. Two-point step size gradient methods. IMA J Numer Anal 1988;8(1):141–8.
[45] Bitzek Erik, Koskinen Pekka, Gähler Franz, Moseler Michael, Gumbsch Peter. Structural relaxation made simple. Phys Rev Lett 2006;97(17):170201.
[46] Schaefer S, Fierro V, Szczurek A, Izquierdo MT, Celzard A. Physisorption, chemisorption and spill-over contributions to hydrogen storage. Int J Hydrog Energy 2016;41(39):17442–52.
[47] Liu Zizhong, Chen Xihao, Liao Yuehong, Zhang Longxin, Laranjeira José AS. First-principles insights of na-decorated B7N5 monolayer for advanced hydrogen storage. Surfaces Interfaces 2025;58:105802, URL https://www.sciencedirect.com/science/article/pii/S2468023025000653.
[48] Martins Nicolas F, Maia Ary S, Laranjeira José AS, Fabris Guilherme SL, Albuquerque Anderson R, Sambrano Julio R. Hydrogen storage on the lithium and sodium-decorated inorganic graphenylene. Int J Hydrog Energy 2024;51:98–107, URL https://www.sciencedirect.com/science/article/pii/S0360319923055398.
[49] Othman Wael, Alfalasi Wadha, Hussain Tanveer, Tit Nacir. Light-metal functionalized boron monoxide monolayers as efficient hydrogen storage material: Insights from DFT simulations. J Energy Storage 2024;98:113014.
[50] Duan Zhanjiang, Shi Shunping, Yao Chunyu, Liu Xiaoling, Diao Kai, Lei Dan, Liu Yiliang. Reversible hydrogen storage with na-modified irida-graphene: A density functional theory study. Int J Hydrog Energy 2024;85:1–11.
[51] Chen Xihao, Li Jiwen, Zhang Longxin, Wang Ning, Cheng Jiang, Ma Zhenyu, Gao Peng, Wang Guangzhao, Cai Xinyong, Guo Donglin, Xiang Jing, Zhang Liang. Computational evaluation of Li-decorated α-C3N2 as a room temperature reversible hydrogen storage medium. Int J Hydrog Energy 2024;62:510–9, URL https://www.sciencedirect.com/science/article/pii/S0360319924009212.
[52] Chen Xihao, Zhang Liang, Jia Huaijie, Gao Peng. Computational investigation of a reversible energy storage medium in g-B5N3 decorated by lithium. Langmuir 2024;40(22):11582–9, arXiv:https://doi.org/10.1021/acs.langmuir.4c00779. PMID: 38785077.
[53] Vaidyanathan Antara, Kandasamy Manikandan, Ramaniah Lavanya M, Wagh Vaibhav, Chakraborty Brahmananda. Hydrogen storage in Sc-decorated ψ-graphene via density functional theory simulations. Int J Hydrog Energy 2024;52:376–89, URL https://www.sciencedirect.com/science/article/pii/S0360319923045500.
[54] Laranjeira José AS, Martins Nicolas F, Ye Lingyu, Sambrano Julio R, Chen Xihao. Hydrogen storage engineering in PHE-graphene monolayer via potassium (K) decoration. Int J Hydrog Energy 2025;123:139–49, URL https://www.sciencedirect.com/science/article/pii/S0360319925014235.
[55] Wang Qing, Sun Huilin, Li Qingyu, Yang Xiao, Chen Wei, Yan Jing, Lyu Yanfeng, Yan Gang, Zhao Huaihong, Meng Zhaoshun, et al. Enhanced hydrogen storage in K and Na decorated DHP-graphene monolayer: DFT and GCMC study. Chem Phys Lett 2025;141932.
[56] Chen Xihao, Zhang Che, Liu Zonghang, Li Jiwen, Guo Donglin, Zhang Liang, Cheng Jiang, Zhang Longxin, Wang Guangzhao, Gao Peng. First-principles investigation of high reversible energy storage medium in Li-decorated net-Y. J Energy Storage 2024;103:114445, URL https://www.sciencedirect.com/science/article/pii/S2352152X24040313.
[57] Chen Xihao, Wang Jiazhuo, Martins Nicolas F, Sambrano Julio R, Laranjeira José AS. Penta-octa B4C2N3: A new 2D material for high-performance energy applications. Langmuir 2025.
[58] Kumar Narender, Sharma Munish, Pandey Ravindra, Tit Nacir. Borophene/graphene heterostructure for effective hydrogen storage with facile dehydrogenation. Int J Hydrog Energy 2024;70:510–21, URL https://www.sciencedirect.com/science/article/pii/S0360319924017543.
[59] Mane Pratap, Kaur Surinder Pal, Singh Mukesh, Kundu Ajit, Chakraborty Brahmananda. Superior hydrogen storage capacity of vanadium decorated biphenylene (Bi+V): A DFT study. Int J Hydrog Energy 2023;48(72):28076–90, URL https://www.sciencedirect.com/science/article/pii/S0360319923017408.
[60] DOE technical targets for onboard hydrogen storage for light-duty vehicles. 2025, https://www.energy.gov/eere/fuelcells/doe-technical-targets-onboard-hydrogen-storage-light-duty-vehicles. [Accessed June 2025].